ELSEVIER

Nuclear Instruments and Methods in Physics Research A 466 (2001) 126–141

NUCLEAR INSTRUMENTS & METHODS IN PHYSICS RESEARCH Section A

www.elsevier.nl/locate/nima

Thin-film-coated bulk GaAs detectors for thermal and fast neutron measurements

D.S. McGregor[a,*], R.T. Klann[b], H.K. Gersch[a], Y.H. Yang[a]

[a] *Department of Nuclear Engineering and Radiological Sciences, University of Michigan, 2355 Bonisteel Boulevard, Ann Arbor, MI 48109-2104, USA*

[b] *Argonne National Laboratory, 9700 South Cass Avenue, Argonne, IL 60439, USA*

Abstract

GaAs-based structures are presently under investigation as the substrate for ^{10}B-coated and polyethylene-coated neutron detectors. The semi-insulating (SI) GaAs-based devices operate at low bias voltages by employing the truncated electric field effect, which allows for acceptable signals to be produced with bias voltages ranging between 10 and 50 V. At this time, the ^{10}B-coated devices have demonstrated over 3.5% intrinsic thermal neutron detection efficiency with reactive films 1.8 μm thick. Relatively high neutron/γ-ray rejection ratios can be achieved with an appropriate choice of lower level discriminator setting. Polyethylene-coated GaAs devices are being studied as fast neutron detectors and have shown evidence of (n,p) reactions for 14 MeV neutrons. Theoretical neutron responses and experimental neutron detection data are presented and compared.

Keywords: Neutron detector; Semiconductor detector; Radiation detector; Neutron detection

1. Introduction

Semiconductor particle detectors coated with neutron reactive films have shown promise as potential neutron detectors [1–6]. The device operation is simple and a detailed description is provided in the literature [5,7]. Briefly stated, a semiconductor diode detector is coated with a neutron reactive film that spontaneously emits ionizing radiation upon the absorption of a neutron. The ionizing radiation, preferably in the form of charged particles, can enter the diode detectors and be detected.

Generally, the methods used to recognize neutron interactions within a detector rely on second-order effects. Two very common neutron interactions that are used for a variety of *thermal* neutron detectors are the ^{10}B(n,α)^{7}Li reaction [1,5] and the ^{6}Li(n,α)^{3}H reaction [6,8]. The charged-particle reaction products emitted as a result of neutron interactions in ^{10}B and ^{6}Li can be easily detected with a charged-particle detector. Low atomic number materials such as hydrogen tend to have relatively high elastic scattering cross sections for fast neutrons, and often (n,p) reactions from fast neutrons interacting in hydrogen-filled materials are manipulated for *fast* neutron detection. High-density polyethylene (HDPE) has a high

*Corresponding author. Tel.: +1-734-647-8964; fax: +1-734-763-4540.
E-mail address: dsmcgreg@umich.edu (D.S. McGregor).

0168-9002/01/$ - see front matter
PII: S0168-9002(01)00835-X

concentration of hydrogen, and energetic recoil protons (hydrogen nuclei) scattered by fast neutrons within the HDPE material can be detected by a charged-particle detector [9–11]. The neutron detector designs discussed in the present article consist of semi-insulating (SI) bulk GaAs Schottky barrier detectors coated with a layer of neutron reactive material. The detectors have been coated with either 98% pure ^{10}B for *thermal* neutron detection or HDPE for *fast* neutron detection.

SI bulk GaAs has been studied as a radiation detector for a variety of applications [12] yet has suffered difficulties due to electric field perturbations in Schottky-based diodes fabricated from the material [12]. Reverse-biased Schottky barrier diodes fabricated from undoped SI GaAs that have been compensated with the deep level EL2 demonstrate an unusually truncated electric field distribution. The electric field in reverse-biased SI GaAs diodes is clearly divided into a high electric field region (approximately 10^4 V/cm) and a low electric field region (negligible voltage) [12–15]. This important discovery demonstrated that, firstly, only a small region near the rectifying contact was actually active under low reverse bias, and secondly, the active region increased in width *linearly* with applied voltage. The active region width increases on an average as 1 V/μm, although the dependence has been observed to range between 0.5 and 2.0 V/μm. Termed the "truncated electric field effect" (TEF effect), the authors find the phenomenon fortuitous in the present case. Under a very low voltage, a thin region of high electric field is confined near the GaAs blocking contact while the remainder of the device is virtually inactive. Since charged particle reaction products from the ^{10}B(n,α)^{7}Li reaction have a range no greater than 5 μm in GaAs, the thin active region is adequate to detect pulses. Due to its small volume, the probability of γ rays interacting in the thin active region is negligible. Also, γ rays interacting within the low electric field region mainly produce small voltage pulses which can be electronically discriminated and rejected. Hence, the TEF effect observed with SI GaAs diodes helps to naturally discriminate between neutron-induced events and background γ-ray events.

2. ^{10}B and ^{6}Li coatings

2.1. ^{10}B coatings

The microscopic *thermal* neutron absorption cross section (σ) for ^{10}B is 3840 b, which is a relatively high value and is one of the main reasons why ^{10}B is used for thermal neutron detection. The microscopic neutron absorption cross section decreases with increasing neutron energy, with a dependence proportional to the inverse of the neutron velocity ($1/v$) over much of the energy range [16,17]. The atomic density for *pure* ^{10}B is 1.3×10^{23} atoms/cm^3, resulting in a macroscopic thermal neutron absorption cross section (Σ) of 500/cm. The ^{10}B(n,α)^{7}Li reaction leads to the following products [18]:

$$^{10}B + {}^1_0\mathrm{n} \rightarrow \begin{cases} {}^7\mathrm{Li}(\text{at } 1.015\ \mathrm{MeV}) + \alpha(\text{at } 1.777\ \mathrm{MeV}), & 2.792\ \mathrm{MeV}\ (\text{to ground state}) \\ {}^7\mathrm{Li}^*(\text{at } 0.840\ \mathrm{MeV}) + \alpha(\text{at } 1.470\ \mathrm{MeV}), & 2.310\ \mathrm{MeV}\ (\text{1st excited state}) \end{cases}$$

(Reaction Q-value)

which are released in opposite directions when thermal neutrons (0.0259 eV) are absorbed by ^{10}B. After absorption, 94% of the reactions leave the ^{7}Li ion in its first excited state, which rapidly de-excites to the ground state ($\sim 10^{-13}$ s) by releasing a 480 keV γ-ray. The remaining 6% of the reactions result in the ^{7}Li ion dropping directly to its ground state.

Either an α-particle or a ^{7}Li ion reaction product may reach the GaAs detector after a ^{10}B(n,α)^{7}Li reaction. If so, the energy registered by the detector is simply the original particle energy minus the energy absorbed in the boron film and detector contact during transit. The device contacts are very thin, and it can

be assumed that energy loss in the detector contact is negligible. At any reaction location within the ^{10}B film, the maximum detector entrance energy will be retained by either particle should it enter the detector in an orthogonal trajectory. For the same interaction distance from the detector, the energy retained by the particle when it reaches the detector decreases as the angle exceeds orthogonality.

The *average* range for a 0.840 MeV ^{7}Li ion *in pure* ^{10}B is 1.6 μm and the *average* range for a 1.47 MeV α-particle *in pure* ^{10}B is 3.6 μm. At the end of the average range, the charged particle no longer has any energy and can not be detected. The longest range that a particle can transit through the reactive film and still retain detectable energy for a given system is referred to as the *effective range*, L [5,7]. Given a predetermined lower level discriminator (LLD) setting, the average *effective* range (L) for either particle can be determined. For example, an LLD setting of 300 keV yields a calculated value of $L_{Li} = 0.810\,\mu m$ for 840 keV ^{7}Li ions and $L_{\alpha} = 2.648\,\mu m$ for 1.47 MeV α-particles [5,7,19]. At 300 keV, the ΣL product for 840 keV ^{7}Li ions is 0.0405, and the ΣL product for 1.47 MeV α-particles is 0.1324 [7].

2.2. Pure ^{6}Li coatings

Pure ^{6}Li can be used as a neutron reactive coating, although its corrosive and reactive nature results in cumbersome handling procedures. The microscopic *thermal* neutron (0.0259 eV) absorption cross section for pure ^{6}Li is 940 b. The microscopic neutron absorption cross section also demonstrates a $1/v$ dependence. The neutron absorption cross section for ^{6}Li remains lower than that of ^{10}B for neutron energies below 100 keV. There is a salient resonance in the ^{6}Li cross section appearing above 100 keV, in which the neutron absorption cross section for ^{6}Li surpasses that of ^{10}B for energies between approximately 150 to 300 keV [16,17]. Pure ^{6}Li has a mass density of $0.463\,g/cm^3$ and an atomic density of 4.634×10^{22} atoms/cm^3. The macroscopic *thermal* neutron absorption cross section is 43.56/cm.

The $^{6}Li(n,\alpha)^{3}H$ reaction leads to the following products::

$$^{6}Li + {}^{1}_{0}n \rightarrow {}^{3}H(\text{at } 2.73\text{ MeV}) + \alpha(\text{at } 2.05\text{ MeV}), \quad \underline{\text{Reaction } Q\text{-value}}\ 4.78\text{ MeV}$$

which are oppositely directed if the neutron energy is sufficiently small. Although the thermal neutron absorption cross section for ^{6}Li is lower than with ^{10}B, the higher reaction product energies make it attractive for thermal neutron detection.

The low atomic density and the low mass density of pure ^{6}Li result in rather large reaction product ranges [7]. With an LLD setting of 300 keV, the values of L for the pure ^{6}Li film far surpass those calculated for the pure ^{10}B film, with $L_{\alpha} = 19.05\,\mu m$ and $L_{H} = 126.77\,\mu m$. Also, the resulting ΣL products are much greater. At an LLD setting of 300 keV, the 2.73 MeV triton ΣL product is 0.5532 and the 2.05 MeV α-particle ΣL product is 0.0828. Although large, these ΣL values require rather thick reaction product films to achieve optimum performance, which may be difficult to deposit and difficult to prevent from decomposing.

2.3. ^{6}LiF coatings

One popular form of ^{6}Li is the stable compound of ^{6}LiF. The molecular density of ^{6}LiF is 6.118×10^{22} molecules/cm^3, therefore the atomic density of ^{6}Li atoms within ^{6}LiF amounts to the same. The mass density of ^{6}LiF is $2.541\,g/cm^3$. With a microscopic thermal neutron cross section of 940 b for ^{6}Li, the resulting macroscopic thermal neutron cross section for ^{6}LiF is 57.51/cm.

An LLD setting of 300 keV gives L_{α} as 4.64 μm and L_{H} as 29.25 μm [7]. At 300 keV, the ΣL product for 2.05 MeV α particles is 0.0267 and the ΣL product for 2.73 MeV tritons is 0.1682. The ΣL products for ^{6}LiF are very similar to those of pure ^{10}B, indicating that their maximum achievable thermal neutron efficiencies should also be similar.

2.4. Theoretical efficiency for frontal irradiation

It can be shown that the neutron detection efficiency is [5,7]

$$S_p(D_F) = \frac{F_p}{4\pi I_0}\int_0^{D_F} I_0 2\pi\Sigma_F e^{-\Sigma_F(D_F-x)}\left(1-\frac{x}{L}\right)dx = 0.5F_p\left\{\left(1+\frac{1}{\Sigma_F L}\right)(1-e^{-\Sigma_F D_F}) - \frac{D_F}{L}\right\} \quad (1)$$

for $D_F \leqslant L$, and

$$S_p(D_F) = \frac{F_p e^{-\Sigma_F(D_F-L)}}{4\pi I_0}\int_0^{L} I_0 2\pi\Sigma_F e^{-\Sigma_F(D_F-x)}\left(1-\frac{x}{L}\right)dx = 0.5F_p e^{-\Sigma_F(D_F-L)}\left\{\left(1+\frac{1}{\Sigma_F L}\right)(1-e^{-\Sigma_F L}) - 1\right\} \quad (2)$$

for $D_F > L$, where I_0 is the initial neutron beam intensity, D_F is the reactive film thickness and F_p refers to the branching ratio of the reaction product emission. The total efficiency can be found by summing each of the reaction product efficiencies:

$$S(D_F)|_{Total} = \sum_{p=1}^{N} S_p(D_F), \quad (3)$$

where N is the number of possible reaction product emissions at different energies. In the case of ^{10}B-based films, N equals 4 whereas for ^{6}Li-based films, N equals 2. Notice from Eq. (2) that the value of S_p decreases as D_F exceeds the value of L. Films thicker than L for the long-range reaction product serve to only absorb neutrons without increasing the detection efficiency. The efficiency decreases with increasing film thickness because neutrons are absorbed in the outermost film layer without the charged-particle reaction products reaching the detector. The maximum range of the charged particles in addition to the neutron cross section will set an absolute limit on the intrinsic efficiency of the detector. As a result, there will be an optimal neutron reactive film thickness for frontally irradiated detectors. Since the minimum particle detection threshold determines the average effective range (L), the optimal film thickness is also a function of the LLD setting [5,7].

Using a LLD setting of 300 keV, Figs. 1 and 2 show the expected thermal neutron detection efficiency for ^{10}B, ^{6}LiF, and pure ^{6}Li films as a function of film thickness. Note from Fig. 1 that only a slight gain is achieved in detection efficiency by using ^{6}LiF (4.3%) instead of ^{10}B (4%), yet the ^{6}LiF film thickness

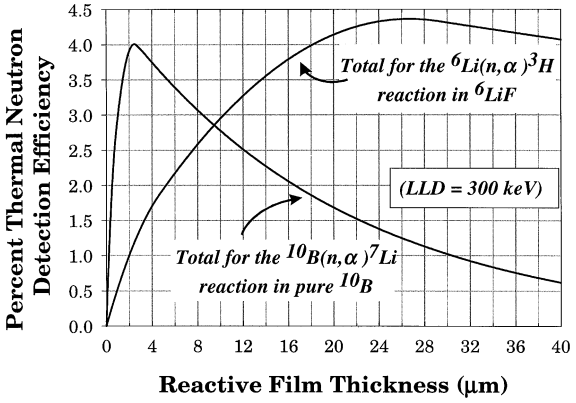

Fig. 1. Theoretical thermal neutron detection efficiency for ^{10}B-coated and ^{6}LiF-coated semiconductor detectors. The curves shown are for frontal irradiation with a LLD setting of 300 keV.

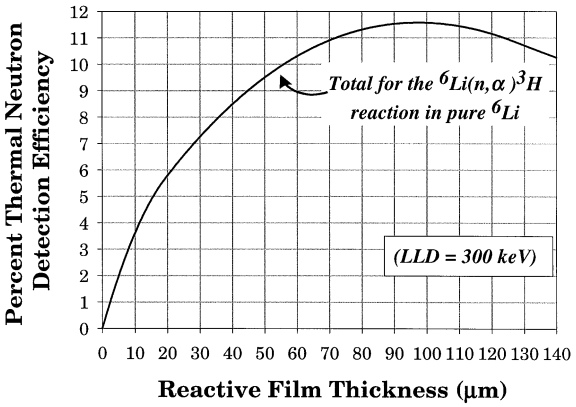

Fig. 2. Theoretical thermal neutron detection efficiency for pure ^{6}Li-coated semiconductor detectors. The curve shown is for frontal irradiation with a LLD setting of 300 keV.

required to *match* the efficiency achieved with ^{10}B is almost 8 *times greater*. Due to thin-film stress-related problems in ^{6}LiF, the authors have chosen to use ^{10}B. Fig. 2 shows the expected efficiency for pure ^{6}Li films with a LLD setting of 300 keV. With a maximum efficiency of 11.6% for thermal neutron detection, pure ^{6}Li films can clearly outperform ^{10}B and ^{6}LiF films. However, the ^{6}Li film thickness required to match the performance of ^{10}B is approximately 5 times greater, and the optimum performance is achieved with a film thickness of approximately 95 μm. For frontal irradiation of thin-film-coated devices, the optimum film thicknesses for each are apparent in Figs. 1 and 2 and require the careful control of film deposition and final thickness. Methods exist, however, to remedy those difficulties so that stringent control can be relaxed in conjunction with increased thermal neutron detection efficiency [7].

3. HDPE-coated detectors

HDPE-coated detectors are sensitive to recoil protons produced from elastic scattering in the hydrogen. Although ^{10}B has a large thermal neutron cross section, it has a much lower neutron cross section for epithermal and fast neutrons. On the other hand, hydrogen-filled materials can be used to produce energetic protons through elastic scattering. The scattering cross section for hydrogen is larger than the absorption cross section for ^{10}B for neutron energies above 1 keV, but it is much lower than the absorption cross section for ^{10}B for neutron energies below 1 keV.

For fast neutrons (neutrons exceeding of 500 keV), a hydrogen-rich coating such as HDPE will produce relatively good detection efficiency. The recoil proton energy is dependent on the initial neutron energy [11]. A simple code was written to examine simultaneously the behavior of the HDPE coating and the proton energy loss in both the HDPE the GaAs detector active region [11]. The fast neutron cross section for scattering is very low, therefore the addition of thin HDPE layers on the detector do not significantly degrade the neutron beam. The intrinsic efficiency was calculated as a function of neutron energy for different coating thicknesses, the results of which are discussed elsewhere [11]. It was found that maximum efficiency for 14 MeV neutrons was limited to HDPE films of 2200 μm thickness. This is reasonable since it corresponds to the maximum range of a 14 MeV proton in HDPE. The recoil protons cannot reach the active region of the detector when interactions in the coating occur more than 2200 μm away.

The expected detection responses from a variety of HDPE film thicknesses were analyzed, and it was observed that the spectral response of the detector can be tailored by varying the HDPE coating thickness

[11]. For any given neutron energy, the detector efficiency is maximized for a coating thickness that matches the maximum range of a proton with the same energy. This would occur for a scattering event in which the proton was ejected at a zero degree angle or directly forward. Similar to the cases with ^{10}B- and ^{6}Li-based films, the maximum range of the charged particle coupled with the neutron cross section will set an absolute limit on the intrinsic efficiency of the detector.

Directional dependence of the HDPE-coated detectors is readily apparent from the kinematics of elastic scattering from hydrogen. Recoil protons do not scatter in the backward direction. Furthermore, the proton energy is a strong function of the scattering angle. A neutron transfers all of its energy to forward-scattered (0°) protons and transfers none of its energy to 90° scattered protons. No detectable response is expected if a detector is placed backward in a neutron beam so that the HDPE-coated surface points away from the neutron source. The detectors should perform as directionally sensitive devices.

4. Basic device structure and fabrication steps

The GaAs devices were fabricated from 75 mm diameter, 600 μm thick, low-etch-pit density, vertical-gradient-freeze (VGF) grown, SI bulk GaAs wafers acquired from American X-tal Technologies. Processing began by first lapping 150 μm of material off of one side of the wafers with a slurry composed of 3 μm Al_2O_3 powder and de-ionized (DI) water. Throughout the entire fabrication process described as follows, only 18-MΩ DI water was used. Polishing was performed in two steps: intial polishing was performed with a solution of $NaH_2PO_2 \cdot H_2O$ and 0.3 μm Al_2O_3 powder, followed by a chemo-mechanical polishing step with a 1 : 250 : 250 solution of $Br : CH_3OH : HOCH_2CH(OH)CH_2OH$. The samples were then cleaned in a series of solvents followed by a water wash. Etching proceeded for 5 min in a dilute solution of 1 : 1 : 320 $H_2SO_4 : H_2O_2 : H_2O$ followed by a 2 min water cascade rinse. A final 1 : 1 $HCl : H_2O$ oxide removal step was used, followed by a H_2O rinse and gaseous N_2 drying procedure. An evaporator was used to coat the polished surface with Au/Ge/Ni layers [20]. To reduce the contact resistance, the Au/Ge/Ni layers were sintered at 400°C in a gaseous Ar environment for duration of 1 min.

The front sides of the wafers were then lapped and polished again as previously described, resulting in an overall wafer thickness of 200 μm. The samples were cleaned and etched also as previously described. The devices were patterned with 3.5-mm diameter openings for image reversal photoresist "liftoff". The open areas were cleaned for 2 min in an oxygen plasma, followed by a final 1 : 1 $HCl : H_2O$ oxide removal step. The wafers were rinsed for 2 min in a water cascade and dried with an N_2 (g) shower. A very thin layer of Ti/Au (150 Å/400 Å) was evaporated over the wafer and lifted off. Circular 3-mm diameter photoresist patterns were centered over the Schottky contacts. The open phototresist patterns were cleaned in an oxygen plasma. Afterwards, 98% purified ^{10}B was evaporated over the Schottky contacts and defined by a conventional liftoff process. A variety of samples were processed, and the ^{10}B films ranged in thickness between 1000 and 18 400 Å.

HDPE-coated devices were similarly fashioned. The exceptions to note are that the boron evaporation step was not performed and the active Schottky contact regions had diameters of 5.6 mm rather than 3.5 mm. A spray adhesive was applied to adhere 5.6 mm diameter circles of HDPE to the Schottky contacts of the devices. The HDPE disks ranged in thickness from 50 μm up to 2 mm.

Ti/Au contacts were evaporated upon 1 mm thick Al_2O_3 substrate holders. To reduce effects from scattered neutrons, the substrate holders were designed with a centered hole slightly larger than the GaAs detector Schottky contact patterns. A layer of Ti/Au was evaporated along the perimeter of the hole, and the bulk GaAs devices were centered over the hole with the Schottky contact facing away from the Al_2O_3 substrate holder. The low resistance contact (anode) was bonded to the annular Ti/Au contact around the hole with silver epoxy. The basic configurations for the ^{10}B-coated and

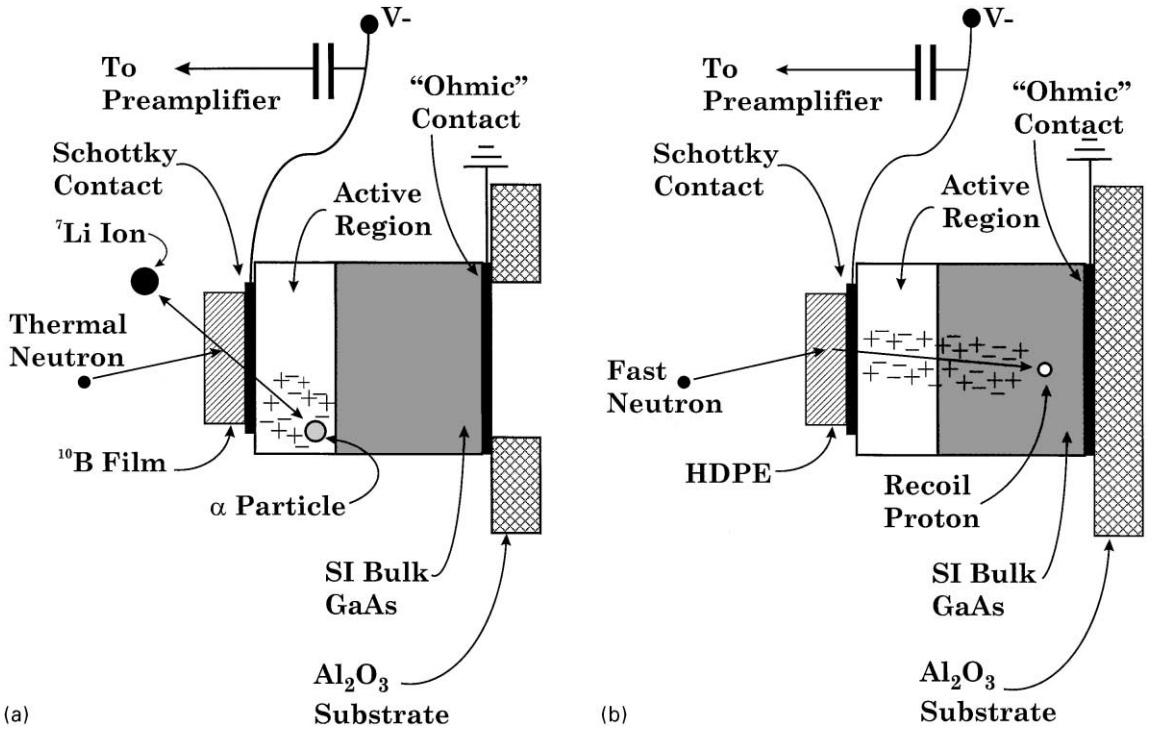

Fig. 3. The basic configurations for the (a) ^{10}B-coated SI bulk GaAs detectors and (b) the HDPE-coated SI bulk GaAs detectors. The HDPE-coated devices are operated with the coated side facing the neutron beam, whereas the ^{10}B-coated devices were operated in either direction.

HDPE-coated devices can be seen in Fig. 3. Devices coated with ^{10}B were operated with either contact surface facing the neutron source, whereas HDPE devices were operated primarily with the coated surface facing the neutron source.

5. Results from ^{10}B-coated devices

The mounted devices were installed into aluminum testing boxes designed to reduce radiofrequency (RF) and photoelectric noise [19]. The boxes have two cylindrical, close-ended, hollow chimneys opposite each other on the front and on the back. The chimney box design enables repeatable indexing of the detectors by ensuring a standardized and fixed location in the thermal neutron beam. Each detector was mounted in order that the Schottky contact was centered relative to the hollow chimneys and furthermore that the detector plane was centered within the chimney box. The closed, light impenetrable box was inserted into a HDPE collar that fit snugly into the receiving end of the neutron beam port collimator block. The detector was connected through the aluminum box to an Ortec 142A preamplifier. The signals were shaped in an amplifier and recorded on a multichannel analyzer. One-hour duration measurements were performed, and the dead time was adjusted and maintained at 2%.

The Ford Nuclear Reactor, a 2 MW research reactor, supplied the source of neutrons. The neutron detection efficiency measurements were performed with a beam port (A-port) that did not point towards the reactor; this configuration helped to reduce γ-ray background. Neutrons were moderated through a D_2O

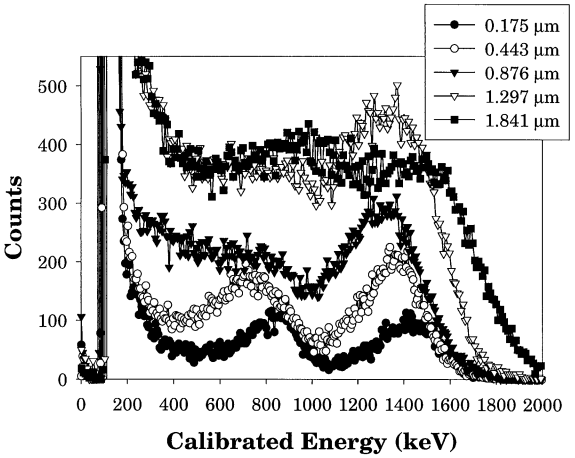

Fig. 4. Spectra taken with ^{10}B-coated SI bulk GaAs detectors of neutron reactions. The data shows the detector response for frontal exposure to a doubly- diffracted thermal neutron beam ($\Phi = 2.7 \times 10^4$ n/cm^2 s). The spectral changes as a function of ^{10}B thickness are apparent. Energy peak resolution is best for thin ^{10}B films, whereas efficiency is highest for the thickest ^{10}B films. All spectra represent 1 h long measurements.

tank, and the thermalized neutron beam was doubly diffracted through two copper plates to further separate the neutrons from γ-ray background [19,21]. The doubly Bragg diffracted neutron beam was then collimated through a HDPE tube to the aluminum chimney box. Before any measurements began, a fission chamber was used to measure the neutron flux emerging from the A-port which gave a value of approximately $\Phi = 2.7 \times 10^4$ n/cm^2 s. Due to control rod movements over the period in which the GaAs neutron detectors were tested, it is expected that the neutron flux value also changed with time. Adjacent beam port experiments also contributed to changes in neutron background. The changes in the neutron flux may amount to a few percent (2–3%), hence the neutron flux value quoted represents only an average measurement.

Detectors with various ^{10}B film thicknesses were tested for both reaction product spectral changes and neutron counting efficiency. Both sides of the detector were tested facing the neutron beam: the Schottky contact side was first tested followed by the ohmic contact side. Although the ohmic contact side did not have a ^{10}B coating on it, thermal neutrons pass through the GaAs detector and still become absorbed in the ^{10}B film [7]. The reaction product emissions were detected as before. The electronics remained unchanged throughout the testing, and all measurements were conducted for a "live time" of 1 h. For the Schottky contact side irradiation, Fig. 4 shows pulse height spectra from ^{10}B(n,α)^{7}Li reactions for ^{10}B films ranging from 1750 Å to 1.84 μm. It is clear that the number of counts under the curves increase with increasing ^{10}B thickness. The reaction products' energy peaks become less distinct with increasing ^{10}B thickness, the expected result of reaction-product energy self-absorption within the ^{10}B film. To illustrate, two distinct energy peaks (840 keV ^{7}Li ion and 1.47 MeV α-article) are present for the 1750 Å coated device, yet neither energy peak is discernable for the 1.84 μm coated device. By summing the number of counts in the channels exceeding 300 keV, the efficiency was determined for several devices as a function of ^{10}B-film thickness for both obverse and reverse irradiations (see Fig. 5). Also shown is the theoretical thermal neutron efficiency curve for an LLD setting of 300 keV, the curve having been calculated from Eq. (1)–(3). Fig. 5 shows good agreement with the developed theory and the measurements. A SI bulk GaAs device (200 μm thick) coated with a 5000 Å layer of ^{10}B was used to demonstrate the count rate as a function of reverse bias voltage (see Fig. 6). Due to the TEF effect observed with SI bulk GaAs, the neutron count rate changes only slightly above 50 V bias, thus showing only a few percent increase in count rate when the bias is increased from 50

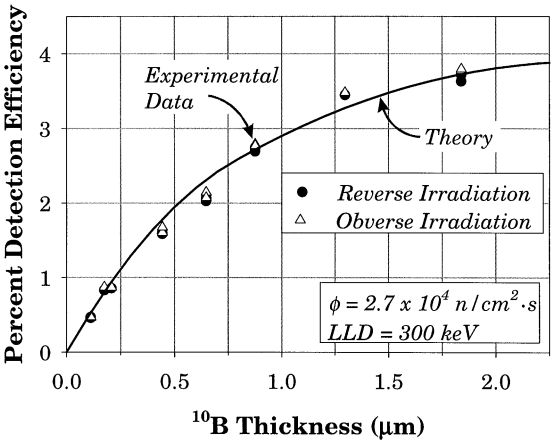

Fig. 5. Thermal neutron detection efficiency for ^{10}B-coated SI bulk GaAs detectors as a function of ^{10}B thickness. The ^{10}B-coated GaAs detectors were irradiated with a doubly-diffracted thermal neutron beam ($\Phi = 2.7 \times 10^4$ n/cm^2 s). The LLD was set at 300 keV equivalent.

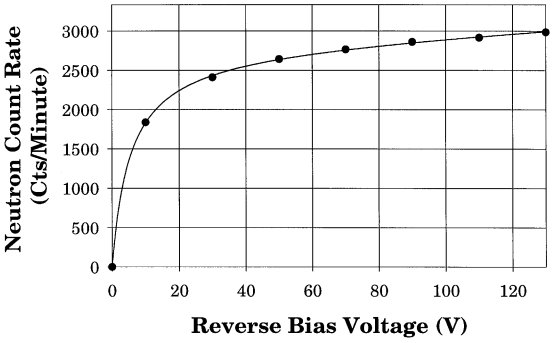

Fig. 6. Count rate as a function of reverse bias voltage for a ^{10}B-coated SI bulk GaAs detector. Due to improving charge collection efficiency, the count rate continued to improve with increasing bias voltage. However, the improvement became minimal for bias voltages above 50 V, showing only a 7.4% increase in count rate for a bias voltage of 130 V.

to 130 V. Spectral changes were apparent, in that the charge collection (and resulting charge induction) increased with the bias voltage [22]. Since the devices are operated as counters and not spectrometers, charge collection efficiency is less important than γ-ray rejection. An increase in bias voltage will increase the detector active region, and will result in more γ-ray background interference. As a consequence, the devices were generally operated with only 50 V bias for the thermal neutron measurements.

Several ^{10}B-coated devices were subsequently placed in the mixed γ-ray and neutron field of a beam port (E-port) that pointed directly at the nuclear reactor core though the D_2O moderator pool. The measured γ-ray component was 1.1 R/h and the neutron flux was approximately $\Phi = 10^6$ n/cm^2 s. Tests were conducted to determine the neutron/γ-ray (n/γ) discrimination ratio as described. Various thicknesses of Pb and Cd were placed between the GaAs detector and the beam port. Lead (Pb) is used to effectively absorb γ rays while permitting a majority of the neutrons to pass through. Cadmium (Cd) is a highly effective absorber of neutrons for energies below 0.5 eV [16,17], and thin sheets of the material (in this case, 5 mm or less) do not significantly reduce the γ-ray background. Prompt γ-ray emissions occur from neutron absorption in Cd [23–25] and some of the γ rays emitted from the Cd will enter the GaAs detector. The γ-ray exposure

decreases inversely with the distance squared ($1/d^2$), and the γ-ray background contamination from (n,γ) reactions in the Cd sheet can be significantly reduced by simply placing the Cd sheets closer to the beam port opening and farther away from the GaAs detector. Otherwise, the γ-ray background would increase and an erroneous measurement of the γ-ray interference emanating from the reactor core would result. For the experiment, a 2 mm Cd sheet was placed in the beam at a distance of 2.5 m away from the detectors, and an additional 3 mm Cd sheet was placed in the beam 1.25 m away from the detectors. Lead (Pb) bricks 5 cm thick, when used, were placed in the neutron beam 10 cm away from the detectors.

The experiment was first conducted by measuring various detectors with the bare beam of mixed γ rays and neutrons. The Cd sheets (5 mm) were placed in the mixed beam to remove the thermal neutron component. Since most of the thermal neutrons have been removed, the resulting spectra are primarily due to γ-ray background from the beam. One can observe the neutron-induced component of the pulse height spectrum by subtracting the Cd attenuated neutron beam spectrum from the bare neutron beam spectrum. The n/γ ratio becomes

$$\frac{\mathrm{n}}{\gamma} \approx \frac{\text{Bare beam counts} - \text{Cd shielded beam counts}}{\text{Cd shielded beam counts}} \approx \frac{(\mathrm{n}+\gamma)-\gamma}{\gamma}. \tag{4}$$

Placing a 5 cm thick Pb brick in the path of the beam effectively reduces the γ-ray component while allowing much of the thermal neutron component to still pass through. The effectiveness of altering the n/γ ratio by Pb shielding was then determined as described. The pulse height spectrum was measured with a 5 cm Pb brick in the path. Afterward, both the 5 mm of Cd sheet and the 5 cm Pb brick are placed in the mixed beam, which yields the remaining γ-ray component. Subtracting the spectra resulting from the combination of Cd and Pb shielding from the Pb-shielded spectra yields the filtered (remaining) neutron component. The neutron component *also* reduces, but not quite as much as the γ-ray component. The new n/γ ratio can be found:

$$\left.\frac{\mathrm{n}}{\gamma}\right|_{5\text{ cm Pb}} \approx \frac{5\text{ cm Pb shielded beam counts} - (\text{Cd} + 5\text{ cm Pb shielded beam counts})}{\text{Cd} + 5\text{ cm Pb shielded beam counts}}. \tag{5}$$

Fig. 7 shows spectra taken with a GaAs diode coated with 8750 Å of ^{10}B. The bulk SI GaAs diode was biased at 50 V for all measurements. Both the ^{7}Li-ion distribution and the α-particle peak are apparent,

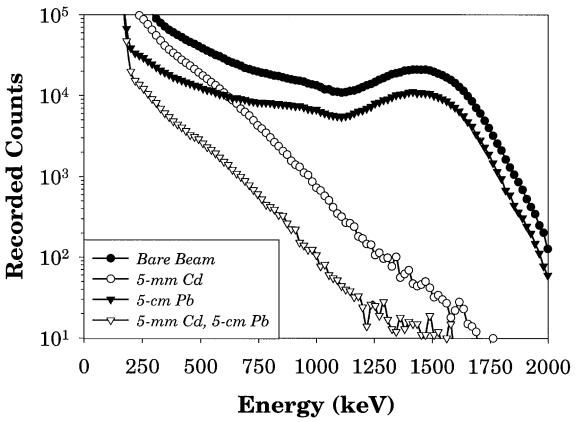

Fig. 7. Comparison spectra of a mixed γ-ray (1.1 R/h) and thermal neutron beam ($\Phi = 2 \times 10^6$ n/cm^2 s). The spectra were taken with a ^{10}B-coated (8750 Å) SI bulk GaAs detector. Shown are spectra with no shielding (bare beam), 5 mm of Cd, 5 cm of Pb, and combined 5 mm of Cd and 5 cm of Pb. The main features of the ^{10}B(n,α)^{7}Li reaction products are apparent in the Pb-filtered and unfiltered spectra but are not observed for the Cd-shielded spectra. Thermal neutrons and γ-rays are both attenuated by the Pb shielding, however the figure shows that a higher percentage of γ-rays are removed than neutrons.

although γ-ray interference distorts and obscures the ^{7}Li ion distribution. The 5 mm Cd shielding effectively removes the neutron-induced portion of the spectrum, resulting in the γ-ray induced spectrum. From Fig. 7, it is apparent that Pb shielding reduces both the neutron interaction rate and the γ-ray interaction rate. However the γ-ray spectrum is reduced by a factor of approximately 6.4 while the neutron spectrum is reduced by a factor of approximately 2.2 (an increase of 2.9 for the n/γ ratio). Fig. 8 shows a comparison of the bare beam spectrum, the spectrum of the Cd-attenuated beam, and the subtracted spectrum. The expected ^{10}B(n, α)^{7}Li reaction product spectrum is clearly shown by subtracting the Cd-shielded spectrum from the bare beam spectrum. Fig. 9 shows a comparison of spectra from 5 cm Pb shielding, combined 5 mm Cd and 5 cm Pb shielding, and the resulting subtracted spectrum. The expected ^{10}B(n, α)^{7}Li reaction product spectrum is observable in the 5 cm Pb-shielded spectrum and is clearly shown by subtracting the Cd-shielded spectrum from the Pb-shielded spectrum.

The peak channel number for the 1.47 MeV α particle was calibrated relative to the channel number of the spectra shown in Figs. 8 and 9. The n/γ ratio was determined as a function of the LLD setting with Eqs. (4) and (5). The results are shown in Fig. 10. The γ-ray field of 1.1 R/h causes background counts to be

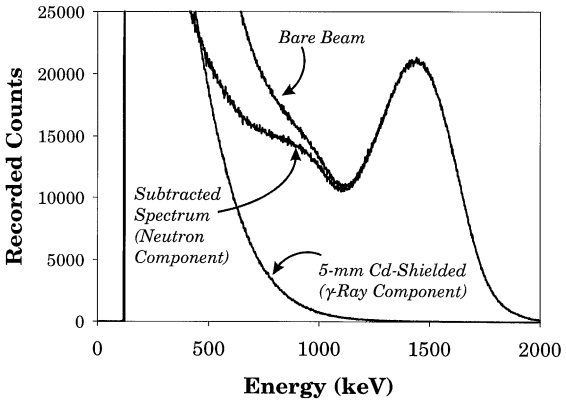

Fig. 8. Comparison spectra of a mixed γ-ray (1.1 R/h) and thermal neutron beam ($\Phi = 2 \times 10^{6}$ n/cm^{2} s). The spectra were taken with a ^{10}B-coated (8750 Å) SI bulk GaAs detector. Shown are spectra with no shielding (bare beam), 5 mm of Cd, and the subtracted spectrum revealing the neutron-induced counts from the bare beam.

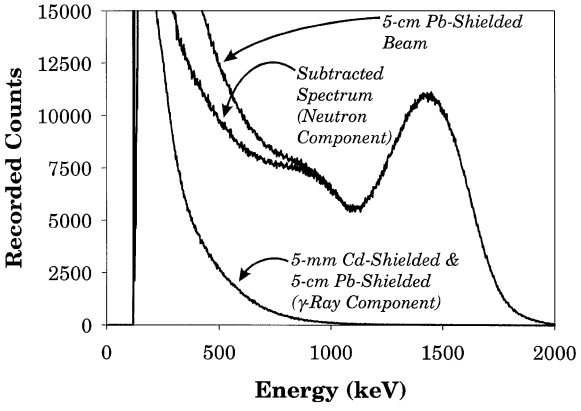

Fig. 9. Comparison spectra of a mixed γ-ray (1.1 R/h) and thermal neutron beam ($\Phi = 2 \times 10^{6}$ n/cm^{2} s). The spectra were taken with a ^{10}B-coated (8750 Å) SI bulk GaAs detector. Shown are spectra with 5 cm of Pb shielding, combined 5 mm of Cd and 5 cm of Pb shielding, and the subtracted spectrum revealing the neutron-induced counts remaining from the Pb shielding.

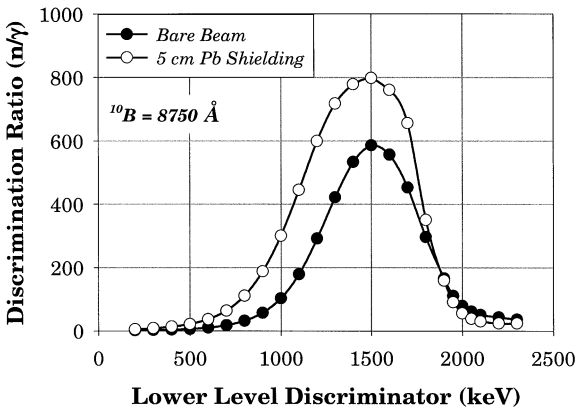

Fig. 10. Experimentally determined n/γ ratios for a ^{10}B-coated (8750 Å), 200 μm thick SI bulk GaAs Schottky barrier detector. The ratio becomes very large as the LLD setting is increased. The figure shows that Pb shielding can increase the n/γ ratio significantly.

registered, yet from Figs. 8 and 9, the γ-ray spectrum is quite different from the neutron-induced spectrum. The n/γ ratio is only 2.47 for the bare beam condition at a LLD setting of 300 keV. As the LLD is increased, fewer γ-ray and thermal neutron induced counts are recorded. It is important to note that the γ-ray distribution is composed primarily of Compton scattering events, hence it is a negatively decreasing exponential, whereas the neutron-induced spectrum is a charged-particle spectral distribution. As a result, the number of γ-ray counts excluded from the measurement dramatically decreases as the LLD is increased, however the number of thermal neutron-induced counts gradually decreases. Fig. 10 shows that the n/γ ratio has a maximum in the distribution, and for this detector the maximum was n/γ = 585 at a LLD setting of approximately 1500 keV. By shielding the device with 5 cm of Pb, the maximum n/γ ratio is increased to 798 at a LLD of 1500 keV. The high LLD setting is due to the energy spread in the 1.47 MeV α-particle peak, within which the thermal neutron–induced counts begin to diminish rapidly beyond this energy. On the other hand, there is a significant disadvantage to setting the LLD at such a high point. Fig. 11 shows the measured neutron detection efficiency as a function of LLD setting and demonstrates two very important points. First, the thermal neutron detection efficiency diminishes with increasing LLD [5]. Second, Pb

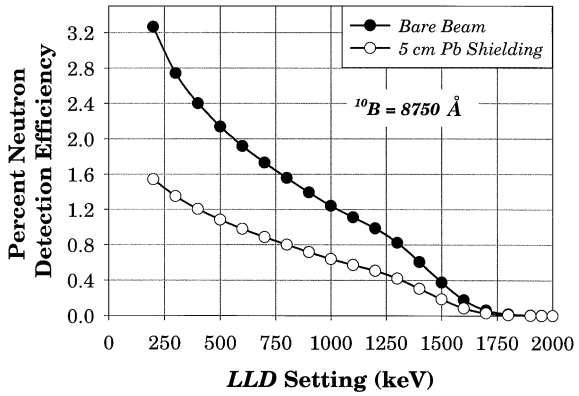

Fig. 11. Experimentally determined thermal neutron detection efficiencies for a ^{10}B-coated (8750 Å), 200-μm thick SI bulk GaAs Schottky barrier detector. The neutron detection efficiency decreases as the LLD setting is increased. Lead (Pb) shielding reduces the neutron detection count rate.

shielding helps to increase the n/γ ratio but works to *decrease* the neutron flux, thereby reducing the neutron count rate. The measurement system can be optimized by selecting a n/γ rejection ratio and then adjusting the LLD so that the highest possible neutron flux (and count rate) is achieved. Shielding with Pb should be used primarily when a n/γ rejection ratio greater than that achievable with a bare beam is required.

6. Results from polyethylene-coated devices

Fast neutron measurements were performed using a MF Physics Model A-711 neutron generator which produces 14 MeV neutrons from D–T reactions. The original output of the neutron generator was recorded at 3×10^{10} n/s, however the device has approximately 200 h of operation on the tube. Therefore, the exact neutron output of the device is unknown, making it difficult to determine the fast neutron detection efficiency. The detectors were placed approximately 10 cm from the front of the neutron generator tube. The measurement periods for each detector were identical at 120 s. Additionally, the electronic operating conditions were unchanged for each measurement with the detectors all biased at 120 V.

A comparison between the detection response for a bare detector and a 125 μm HDPE-coated detector is shown in Fig. 12. As expected, the bare detector shows only γ-ray background from the generator. With the 125 μm HDPE-coated device facing towards the generator, a definite recoil proton spectrum appears [11]. To demonstrate that the device was sensing forward scattered recoil protons, it was turned backwards to the generator, in which the data clearly shows a similar response to the bare detector. As expected, the HDPE-coated GaAs devices are directionally sensitive to fast neutrons [9,11].

Fig. 13 shows a comparison between a bare detector, a detector coated with 125 mm of HDPE, and a detector coated with 875 mm of HDPE. The spectral response for the HDPE-coated devices is similar, an expected result since the initial neutron spectrum from the generator is unchanged [11]. However, the fast neutron detection efficiency is greater for the thicker HDPE film. The total count rate for a detector with 875-μm of HDPE coating was 948 cps, while the total count rate above the "valley"(channel 65) was 504 cps. The total count rate for the detector with a 125-μm HDPE coating was 744 cps, while the total

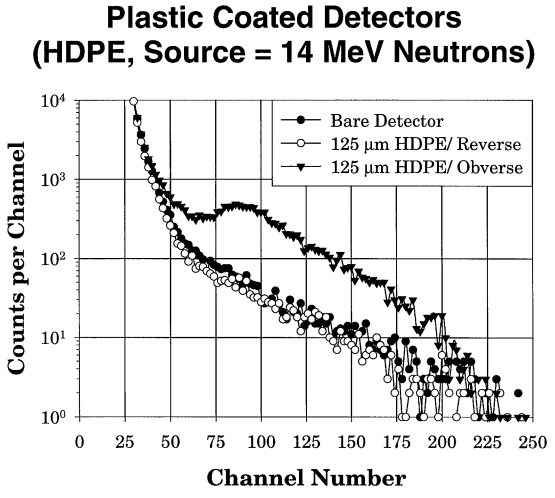

Fig. 12. Comparison spectra taken with HDPE-coated SI bulk GaAs detectors of 14 MeV neutrons from a D–T reaction generator. Shown are spectra with a 125 μm HDPE-coated detector turned reverse (away from the source), turned obverse (towards the source), and an obverse-facing device with *no* HDPE coating for a control reference.

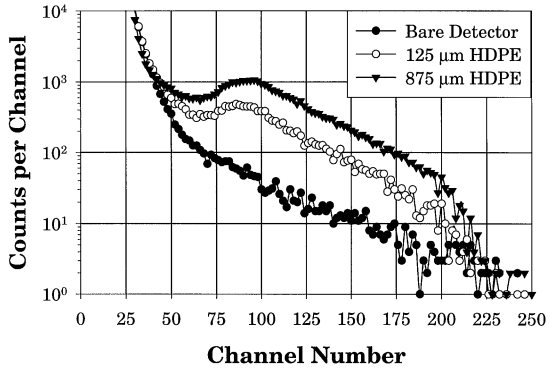

Fig. 13. Comparison spectra taken with HDPE-coated SI bulk GaAs detectors of 14 MeV neutrons from a D–T reaction generator. Shown are spectra taken with a 125 μm coated detector, a 825 μm coated detector, and a device with no coating for reference.

count rate above the "valley" was only 208 cps. Apparently, the counting efficiency does not scale linearly with HDPE thickness, a similar condition found with ^{10}B-coated devices for thermal neutrons.

A SI bulk GaAs device with a 1 μm ^{10}B film coating was placed 10 cm from the front of the neutron generator tube as were the HDPE-coated devices. This allowed for a direct comparison with fast neutron detection for HDPE-coated devices and ^{10}B-coated devices. The entire generator area was surrounded by a significant amount of borated-HDPE (1–2 m) for environmental shielding, hence an abundance of scattered neutrons of lower energy were present. Fig. 14 shows the results from the ^{10}B-coated device, in which a familiar spectrum is observed from the ^{10}B(n, α)^{7}Li reaction for the unshielded case. Afterwards, 19 mm of Pb was placed around the detector to reduce γ-ray background, the result of which is shown in Fig. 14. As can be seen, the spectrum decreased some, yet the count rate remained high. Afterwards, the lead was removed and a sheet of 500-μm thick Cd was placed around the detector to partially remove the scattered low energy (< 0.5 eV) neutron component. The Cd microscopic neutron cross section resonance reduces

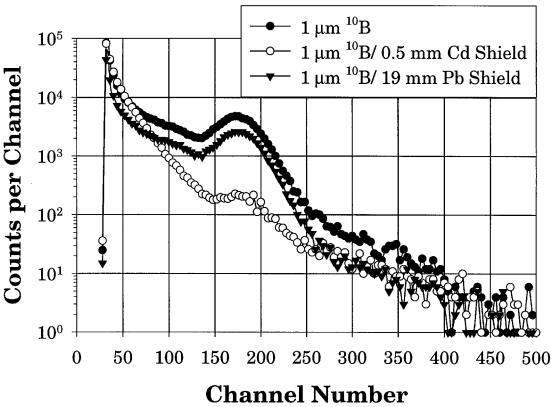

Fig. 14. Comparison spectra taken with a ^{10}B-coated SI bulk GaAs detector within the environment of 14 MeV neutrons from a D–T reaction generator. Shown are spectra taken with a 1 μm coated detector with no shielding, surrounded by Pb shielding, and surrounded by 0.5 mm Cd shielding. The borated-HDPE environmental shielding near the D–T generator scatters neutrons, which are manifested as low energy background neutrons. With Cd shielding the count rate is significantly reduced, showing reduced sensitivity to higher energy (> 0.5 eV) neutrons.

significantly at neutron energies above 0.5 eV [16,17], hence it is expected that the scattered neutrons still reaching the device are primarily of higher energy than 0.5 eV. From Fig. 14, it is easy to see that the count rate reduces significantly. For the Cd-shielded ^{10}B detector, the count rate above the "valley" was only 142 cps, a rate well below that measured for the 875-μm HDPE-coated GaAs detector (504 cps). The authors conclude that HDPE-coated detectors are more sensitive to fast neutrons than the ^{10}B- coated detectors.

7. Conclusions

HDPE-coated and ^{10}B-coated SI bulk GaAs detectors have been used to detect fast and thermal neutrons. The measurements clearly indicate that ^{10}B-coated GaAs detectors can be used in a high γ-ray background environment with a reasonable n/γ rejection ratio. However, the LLD must be increased with increasing γ-ray background, which ultimately reduces the neutron detection efficiency. Additionally, HDPE-coated detectors can be used to detect fast neutrons with higher efficiency than ^{10}B-coated devices can achieve. The HDPE-coated devices have the added advantage that they are directionally sensitive to fast neutrons. Studies are presently underway to determine the radiation hardness and suitability of using SI bulk GaAs devices in harsh radiation environments where neutrons, charged particles, and γ-rays are expected to be present.

Acknowledgements

The presented work was partially funded by the following grants: Argonne National Laboratory Subcontract (DOE) 991262402 and DOE Nuclear Engineering Education and Research Grant DE-FG07-98ID13633. This research was performed under appointment to the US Department of Energy Nuclear Engineering and Health Physics Fellowship Program sponsored by DOE's Office of Nuclear Energy, Science, and Technology.

The neutron detectors were fabricated at the Solid State Electronics Laboratory (SSEL) and the Semiconductor Materials And Radiological Technologies (SMART) Laboratory, both at the University of Michigan. Testing of the devices was performed at the Ford Nuclear Reactor, University of Michigan, and at Argonne National Laboratory. We also recognize Dr. J.T. Lindsay for his cooperation with the experiments.

References

[1] A. Rose, Nucl. Instr. and Meth. 52 (1967) 166.
[2] B. Feigl, H. Rauch, Nucl. Instr. and Meth. 61 (1968) 349.
[3] A. Mireshghi, G. Cho, J. Drewery, T. Jing, S.N. Kaplan, V. Perez-Mendez, D. Wildermuth, IEEE Trans. Nucl. Sci. NS-39 (1992) 635.
[4] R.L. Schulte, F. Swanson, M. Kesselman, Nucl. Instr. and Meth. A 353 (1994) 123.
[5] D.S. McGregor, J.T. Lindsay, C.C. Brannon, R.W. Olsen, IEEE Trans. Nucl. Sci. NS-43 (1996) 1357.
[6] M. Campbell, E.H.M. Heijne, J. Kubasta, P. Middelkamp, S. Pospísil, P. Sícho, W. Snoeys, V. Vrba, Nucl. Instr. and Meth. A 395 (1997) 457.
[7] D.S. McGregor, M.H. Hammig, Y.-H. Yang, H.K. Gersch, Nucl. Instr. and Meth. submitted.
[8] J. Schelten, R. Reinartz, R. Engels, M. Balzhauser, J. Lauter, W. Schafer, K.D. Muller, Nucl. Instr. and Meth. A 389 (1997) 447.
[9] H. Gotoh, H. Yagi, Nucl. Instr. and Meth. 101 (1972) 395.
[10] F. Shirashi, Y. Takami, H. Husimi, S. Ohkawa, C. Kim, Y. Kim, K. Kikuchi, T. Sakai, IEEE Trans. Nucl. Sci. NS-32 (1985) 471.

[11] R.T. Klann, D.S. McGregor, Conference Record of ICONE-8, No. 8110, Eighth International Conference on Nuclear Engineering, April 2–6, 2000, Baltimore, MD, USA.
[12] D.S. McGregor, J.E. Kammeraad, Semiconductors and Semimetals, Vol. 43, Academic Press, San Diego, 1995, p. 383 (Chapter 10).
[13] K. Berwick, M.R. Brozel, C.M. Buttar, M. Cowperthwaite, Y. Hou, Inst. Phys. Conf. Series 135 (1993) 305.
[14] D.S. McGregor, G.F. Knoll, Y. Eisen, R. Brake, Nucl. Instr. and Meth. NS-39 (1992) 1226.
[15] D.S. McGregor, R.A. Rojeski, G.F. Knoll, F.L. Terry Jr., J. East, Y. Eisen, Nucl. Instr. and Meth. A 343 (1994) 527.
[16] D.I. Garber, R.R. Kinsey (Eds.), BNL 325: Neutron Cross Sections, Curves, Vol. 2, 3rd Edition, Brookhaven National Laboratory, Upton, 1976.
[17] V. McLane, C.L. Dunford, P.F. Rose, in: Neutron Cross Sections, Vol. 2, Academic Press, San Diego, 1988.
[18] G.F. Knoll, Radiation Detection and Measurement, 3rd Edition, Wiley, New York, 2000.
[19] D.S. McGregor, S.M. Vernon, H.K. Gersch, S.M. Markham, S.J. Wojtczuk, D.K. Wehe, IEEE Trans. Nucl. Sci. NS-47 (2000), 1364.
[20] D.S. McGregor, G.F. Knoll, Y. Eisen, R. Brake, in: C. del Papa, P.G. Pelfer, K. Smith (Eds.), GaAs Detectors and Electronics for High Energy Physics, World Scientific, Singapore, 1992, p. 30.
[21] D.S. McGregor, J.T. Lindsay, R.W. Olsen, Nucl. Instrum. and Meth. A 381 (1996) 498.
[22] D.S. McGregor, J.T. Lindsay, Y.-H. Yang, J.C. Lee, Conference Record of ICONE-8, No. 8827, Eighth International Conference on Nuclear Engineering, April 2–6, 2000, Baltimore, MD, USA.
[23] M.A. Lone, R.A. Leavitt, D.A. Harrison, At. Data Nucl. Data Tables, 26 (1981) 511.
[24] J.K. Tuli, Thermal Neutron Capture Gamma Rays, BNL-NCS-51647 Report, UC-34-C, Brookhaven National Laboratory, 1983.
[25] J.K. Tuli, in: Z.B. Alfassi, C. Chung (Eds.), Prompt Gamma Ray Activation Analysis, CRC Press, Boca Raton, FL, 1995, p. 177.